ENVIRONMENTAL RESEARCH
LETTERS

LETTER • OPEN ACCESS

Post-drainage vegetation, microtopography and organic matter in Arctic drained lake basins

To cite this article: Juliane Wolter *et al* 2024 *Environ. Res. Lett.* **19** 045001

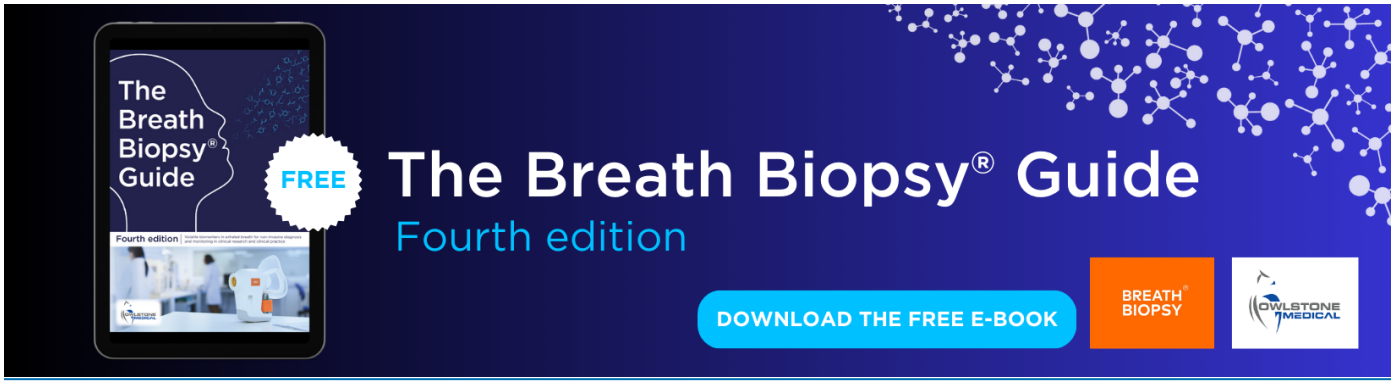

ENVIRONMENTAL RESEARCH
LETTERS

LETTER

Post-drainage vegetation, microtopography and organic matter in Arctic drained lake basins

Juliane Wolter[1,2,*], **Benjamin M Jones**[3], **Matthias Fuchs**[4], **Amy Breen**[5], **Ingeborg Bussmann**[6,7], **Boris Koch**[8], **Josefine Lenz**[2], **Isla H Myers-Smith**[9], **Torsten Sachs**[10], **Jens Strauss**[2], **Ingmar Nitze**[2] and **Guido Grosse**[2,11]

[1] Institute of Biochemistry and Biology, University of Potsdam, Potsdam, Germany
[2] Section Permafrost Research, Alfred Wegener Institute Helmholtz Centre for Polar and Marine Research, Potsdam, Germany
[3] Institute of Northern Engineering, University of Alaska Fairbanks, Fairbanks, AK, United States of America
[4] Renewable and Sustainable Energy Institute, University of Colorado Boulder, Boulder, CO, United States of America
[5] International Arctic Research Center, University of Alaska Fairbanks, Fairbanks, AK, United States of America
[6] Section Shelf Sea System Ecology, Alfred Wegener Institute Helmholtz Centre for Polar and Marine Research, Helgoland, Germany
[7] Section Marine Geochemistry, Alfred Wegener Institute Helmholtz Centre for Polar and Marine Research, Bremerhaven, Germany
[8] Section Ecological Chemistry, Alfred Wegener Institute Helmholtz Centre for Polar and Marine Research, Bremerhaven, Germany
[9] School of GeoSciences, University of Edinburgh, Edinburgh, United Kingdom
[10] Section Remote Sensing and Geoinformatics, GFZ German Research Centre for Geosciences, Potsdam, Germany
[11] Institute of Geosciences, University of Potsdam, Potsdam, Germany
[*] Author to whom any correspondence should be addressed.

E-mail: juliane.wolter.1@uni-potsdam.de

Keywords: tundra vegetation, methane, carbon, nitrogen, remote sensing, machine learning, Teshekpuk lake observatory

Supplementary material for this article is available online

OPEN ACCESS

RECEIVED
26 October 2023

REVISED
12 February 2024

ACCEPTED FOR PUBLICATION
29 February 2024

PUBLISHED
15 March 2024

Abstract

Wetlands in Arctic drained lake basins (DLBs) have a high potential for carbon storage in vegetation and peat as well as for elevated greenhouse gas emissions. However, the evolution of vegetation and organic matter is rarely studied in DLBs, making these abundant wetlands especially uncertain elements of the permafrost carbon budget. We surveyed multiple DLB generations in northern Alaska with the goal to assess vegetation, microtopography, and organic matter in surface sediment and pond water in DLBs and to provide the first high-resolution land cover classification for a DLB system focussing on moisture-related vegetation classes for the Teshekpuk Lake region. We associated sediment properties and methane concentrations along a post-drainage succession gradient with remote sensing-derived land cover classes. Our study distinguished five eco-hydrological classes using statistical clustering of vegetation data, which corresponded to the land cover classes. We identified surface wetness and time since drainage as predictors of vegetation composition. Microtopographic complexity increased after drainage. Organic carbon and nitrogen contents in sediment, and dissolved organic carbon (DOC) and dissolved nitrogen (DN) in ponds were high throughout, indicating high organic matter availability and decomposition. We confirmed wetness as a predictor of sediment methane concentrations. Our findings suggest moderate to high methane concentrations independent of drainage age, with particularly high concentrations beneath submerged patches (up to 200 μmol l^{-1}) and in pond water (up to 22 μmol l^{-1}). In our DLB system, wet and shallow submerged patches with high methane concentrations occupied 54% of the area, and ponds with high DOC, DN and methane occupied another 11%. In conclusion, we demonstrate that DLB wetlands are highly productive regarding organic matter decomposition and methane production. Machine learning-aided land cover classification using high-resolution multispectral satellite imagery provides a useful tool for future upscaling of sediment properties and methane emission potentials from Arctic DLBs.

1. Introduction

Arctic lowlands below 300 m a.s.l. stretch across more than eight million square kilometres of land (Muster *et al* 2017). Such lowlands across Siberia, Alaska, and Canada often have deep ice-rich (Kanevskiy *et al* 2013, Ulrich *et al* 2014) and organic-rich Pleistocene and Holocene permafrost deposits (Hugelius *et al* 2014, Mishra *et al* 2021). These deposits are particularly vulnerable to climatic warming (IPCC 2022) for two reasons: First, increased thaw of ice-rich sediments changes land surface properties, as ice volume loss causes ground subsidence through so-called thermokarst (Kokelj and Jorgenson 2013). Second, rising ground temperatures make large amounts of previously frozen organic matter available for microbial decomposition, potentially enhancing greenhouse gas emissions (Schädel *et al* 2016, Knoblauch *et al* 2018).

Water pooling in thermokarst depressions forms shallow lakes that further enhance thaw along shores and underneath (figure 1(a)) (Langer *et al* 2016). Such lakes may persist for millennia (Edwards *et al* 2016, Fritz *et al* 2016), but thermokarst lake dynamics also include expansion and drainage, resulting in complex mosaics of lakes and DLBs (Grosse *et al* 2013, Jones *et al* 2022). Thermokarst lakes may have perennially thawed zones (taliks) below the water body (figure 1(a)), and old carbon preserved in permafrost for millennia may thaw and decompose (Heslop *et al* 2020). Taliks may therefore release substantial amounts of greenhouse gases (Walter *et al* 2007, Heslop *et al* 2015, Engram *et al* 2020). Eventually, lakes may drain into lower-lying terrain when lake basin sides are breached (Hinkel *et al* 2007), for example through thaw of ice-wedge networks (Mackay 1988) or through coastal erosion (Jones and Arp 2015, Fritz *et al* 2016). In many regions, such as the Arctic Coastal Plain of Alaska, dense mosaics of lakes and DLBs occupy up to 70% of the land surface (Hinkel *et al* 2005, Jones *et al* 2022).

Arctic lowland permafrost affected by lake thermokarst processes has been identified to hold 102 PgC, or 9.5% of the total permafrost carbon pool (Olefeldt *et al* 2016). Drained lake basins (DLBs) largely develop into wetlands (Jorgenson and Shur 2007), and taliks partially or fully refreeze (Ling and Zhang 2004), locking carbon into permafrost. Refreezing, frost cracking, and ice-wedge polygon development start from the first post-drainage winter (Mackay 1999). Over the course of millennia, networks of deep and wide ice wedges develop, thereby strongly altering microtopography. Newly formed hydrological microhabitats from well drained elevated areas to low-lying wet depressions and polygon ponds in turn determine vegetation composition (Wolter *et al* 2016).

Lake drainage provides bare, nutrient-rich ground for pioneer vegetation (figure 1(b)) (Billings and Peterson 1980, Ovenden 1986). With ongoing permafrost aggradation (Mackay 1999, Mackay and Burn 2002) and soil formation (Bockheim *et al* 1999), wetland vegetation transitions from pioneer via fen-type to bog-type wetlands (figure 1(c)) (Treat *et al* 2016). Overall, vegetation succession was studied in very few DLBs in the Arctic, most notably in an artificially drained basin on the Tuktoyaktuk Peninsula in northwestern Canada (Ovenden 1986), on the northern Seward Peninsula in western Alaska (Jones *et al* 2012, Regmi *et al* 2012), and on the Barrow Peninsula in northern Alaska (Billings and Peterson 1980). In newly formed DLBs, sedges in fen vegetation may enhance methane transport from soils to the atmosphere (Verville *et al* 1998, Andresen *et al* 2017), while later on more mature bog vegetation features lower methane emissions (Treat *et al* 2016). Generally, understanding of carbon cycling and methane dynamics in DLB landscapes remains limited due to a scarcity of field data. Some studies investigated ecosystem carbon dynamics from a water table manipulation experiment in a DLB system on the Barrow Peninsula in northern Alaska (Zona *et al* 2009, Sturtevant and Oechel 2013). Other studies compared methane fluxes across lowland tundra landscapes including DLB systems (von Fischer *et al* 2010, Davidson *et al* 2016, Reuss-Schmidt *et al* 2019).

In this study, we used multispectral high-resolution satellite imagery to detect vegetation types in DLBs representing different drainage ages on the Arctic Coastal Plain of Alaska. We hypothesise that vegetation types reflect succession, surface wetness, methane production and sediment type. We propose that this relationship may be used to approximate methane production and sediment properties in Arctic DLBs. Our aim is to understand relationships between vegetation, microtopography, and organic matter in surface sediments and ponds of DLBs. To achieve this goal, we target three main objectives: (1) analyse vegetation and organic matter in surface sediment and ponds along a succession gradient representing different drainage ages, (2) assign vegetation and organic matter parameters to eco-hydrological land cover classes, and (3) quantify the area occupied by different eco-hydrological land cover classes in different drainage age classes in the basins.

2. Study site

Our study site on the Arctic Coastal Plain of Alaska is located just northwest of Teshekpuk Lake (figure 2). The region is characterised by ice-rich (Kanevskiy *et al* 2013) lowland permafrost typical of previously unglaciated northern continental margins from eastern

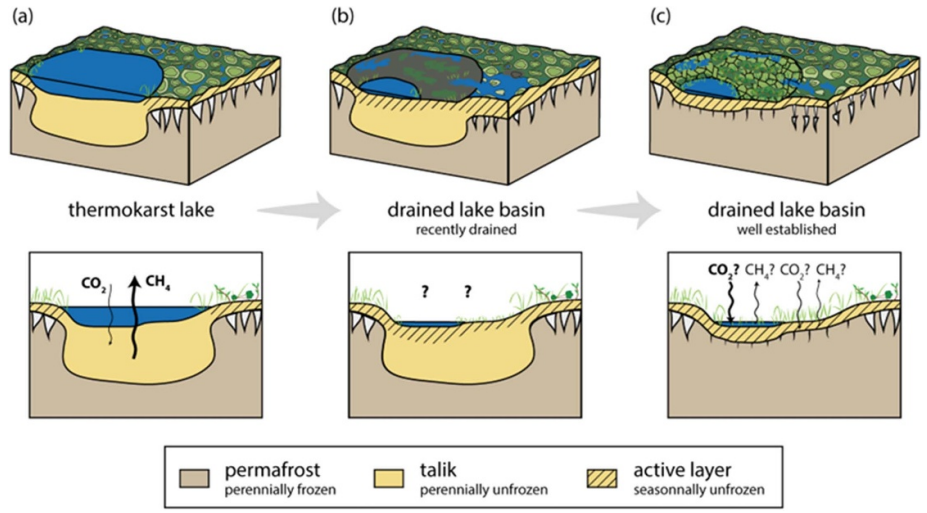

Figure 1. Schematic overview of thermokarst lakes and post-drainage development. The upper panels show surface and sub-surface conditions in a thermokarst lake (a), during the first decades following drainage (b), and finally in a mature drained lake basin (c). The lower panels show associated carbon dynamics.

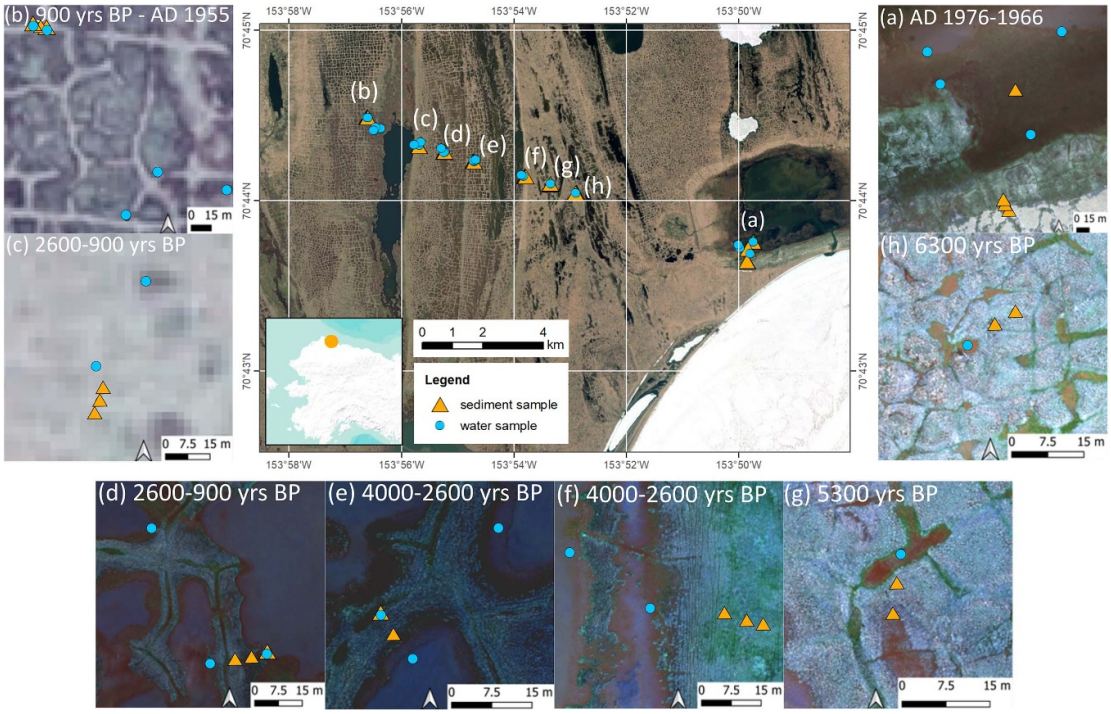

Figure 2. Study area on the Arctic Coastal Plain of Alaska. Sampling sites are indicated as orange triangles (sediment, vegetation and microtopography) and blue circles (water samples). Panels (a)–(h): Sampling sites at each transect location. Note that some lakes are ice covered. Map image source and source of panels (b) and (c): Dynamic Mosaic 2020 Maxar Technologies Inc., Alaska Geospatial Office, USGS. Image source of panels (a) and (d) –(h): Multispectral aerial image orthomosaic (ThawTrendAir 2019 aerial imaging campaign, Rettelbach *et al* 2023).

Siberia to western Canada (Jones *et al* 2022). Lakes and DLBs cover more than 80% of the area north of Teshekpuk Lake (Jones and Arp 2015). Permafrost is continuous and its thickness reaches several hundred metres. Active layer thickness is below 50 cm on average and highly variable (Utqiaġvik region: 10–100 cm, mean 40 cm) (Jafarov *et al* 2017). Climate normals for the periods 1981–2010 and 1991–2020 (ACRC, https://akclimate.org/data/) show an increase of 1 °C in mean annual air temperature to −10.2 °C in Utqiaġvik west of our site and −10.4 °C in Deadhorse to the east. Mean annual precipitation is 137 mm in Utqiaġvik and 145 mm in Deadhorse. The regional vegetation is Arctic tundra.

For this study, we revisited sites for which drainage ages and soil organic carbon stocks are known from previous coring (Fuchs *et al* 2019). These sites were situated along a transect through a large basin

that drained in distinct steps. We covered five drainage stages but could not reach the innermost, youngest drained surface. Therefore, we added a site in a separate nearby basin (figure 2), which drained between 1966 and 1976 based on our visual analysis of Corona satellite photography.

3. Methods

3.1. Field work

We sampled vegetation, surface sediment and pond water around eight transect sites (figures 2 and 3) in early August 2018 to cover the largest possible between-plot variability while still being logistically manageable. At each site, we measured permafrost surface height, ground surface height, and water depth relative to a reference line for each metre along a 10 m sub-transect (S1). At both ends and in the middle of each sub-transect, we surveyed 1 × 1 m vegetation plots using a Braun-Blanquet approach, resulting in 25 vegetation plots. In these plots, we cut ca. 10 × 10 × 3 cm sediment blocks with a knife from just below living vegetation (21 samples). From the same spot, we sampled 2 ml of sediment with a cut-off plastic syringe for methane measurement (21 samples), which we stored in 12 ml glass vials with 2 ml NaOH (1N) to prevent post-sampling methane production.

Additionally, we sampled water from 21 ponds close to the surveyed sub-transects (figure 2), measuring electrical conductivity and pH using a multiparameter probe (WTW Multi 3430 SET F). We filtered dissolved organic carbon (DOC) and total dissolved nitrogen (TDN) subsamples into 20 ml glass vials through 0.7 μm GF/F filters, adding 20–50 μl HCl (30%) to inhibit microbial activity. Subsamples for methane measurement were filled bubble-free into 120 ml glass bottles with 0.3 ml 30% HCl, closed with butyl stoppers and aluminium crimps and stored upside-down to prevent degassing. Water samples were stored cool and arrived in 4 °C laboratory storage within two weeks of sampling.

3.2. Laboratory analyses

We characterised organic matter by measuring total nitrogen (TN), total organic carbon (TOC), stable carbon (δ^{13}C) and nitrogen isotopes (δ^{15}N), and methane (CH_4). We measured TN in an elemental analyser (Elementar rapid MAX N exceed) and TOC in a separate Elementar soliTOC cube. We analysed δ^{13}C (Vienna Pee Dee Belemnite standard) and δ^{15}N (air standard) in an isotope ratio mass spectrometer (Thermo Scientific Delta V Advantage). Methane concentrations were measured with a Shimadzu GC 2014 with FID (Bussmann *et al* 2021), and calculated according to Magen *et al* (2014). DOC and TDN were determined by high temperature catalytic oxidation (HTCO; Shimadzu TOC-VCPN). 6 mL of sample volume were acidified with 0.12 ml HCl (2 mol l^{-1}) and sparged with oxygen (100 ml min^{-1}) for 5 min to remove inorganic carbon, followed by infrared detection of generated CO_2. Total nitrogen was quantified by a chemiluminescence detector (gas flow oxygen: 0.6 l min^{-1}).

3.3. Data analyses

All data analyses were conducted in R (version 4.1.1) (R Core Team 2021). We based our vegetation classification on ordination and clustering of vascular plant and major lichen composition and abundance. Principal component analysis (PCA) and hierarchical clustering were conducted for taxa occurring in at least two plots, using Hellinger transformed vegetation data to reduce rare taxa influence and range transformed environmental data. We correlated organic matter parameters and other environmental variables with PCA results using environmental fitting. Hierarchical clustering used euclidean distances and Ward's D agglomeration. We compared hierarchical clustering against *k*-means clustering and *k*-medoid clustering for two to seven clusters for validation. Boxplots visualised microtopography, sediment and water parameters, comparing drainage age classes as well as moist (water table below ground surface), wet (water table roughly at ground surface, with seasonal variations) and submerged (water table above ground surface) plots. The non-parametric Kruskal–Wallis test and Wilcoxon test aided testing for differences between groups.

3.4. Eco-hydrological land cover classification

We conducted land cover classification using tasseled cap transformed WorldView-2 imagery acquired on 30 July 2014 (ground resolution 2.5 m), which was the best recent mid-summer image. We transformed the raw .ntf files using raster function tools within ArcGIS Pro 3.0.3 and built-in specified parameters for WorldView-2 imagery. Object-based image analysis was conducted on the tasseled cap transformation in eCognition Essentials v. 1.3, using a scaling parameter of 10 to resolve ice wedge polygon terrain features.

We then conducted supervised classification of the image objects using a Bayes classifier in eCognition v. 1.3. Training data was created manually using a multispectral aerial image orthomosaic (RGB and near-infrared) acquired on 23 July 2019 (ThawTrendAir 2019 aerial imaging campaign, 7 cm spatial resolution, Rettelbach *et al* 2023). We created 1400 randomly located points stratified by drainage age class (i.e. 200 points per class) using the 'Random Points in Polygons' tool in QGIS. We created 200 additional random points for the large recently drained basin with its sparse point density and 100 points for Teshekpuk Lake. We used visual expert determination to label random points with target classes. We then performed stratified

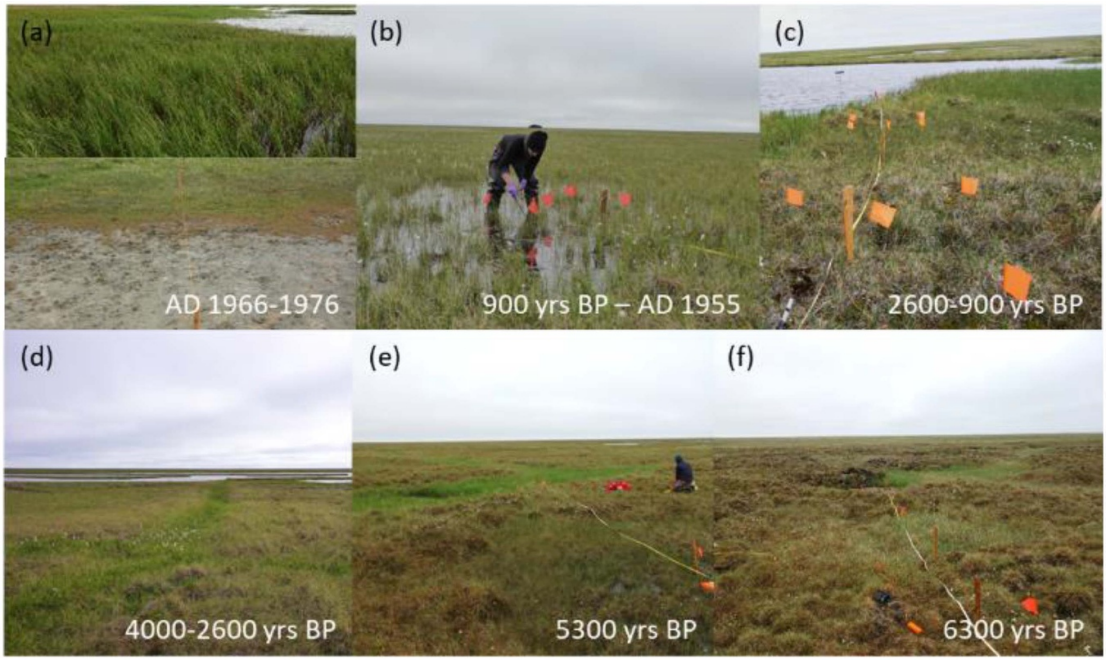

Figure 3. Basin age sequence in photographs. (a) Recently drained (AD 1966–1976) lake basin with large homogeneous vegetation patches and bare ground, (b) drained between 900 yrs BP and AD 1955 with minimal differences in surface height, (c) drained 2600–900 yrs BP, (d) drained 4000–2600 yrs BP, (e) drained 5300 yrs BP, (f) drained 6300 yrs BP.

5-fold cross-validation, splitting the labelled dataset into five equally sized splits with 80% training and 20% validation. All five validation sets add up to the full dataset, enabling a more robust validation than a simple split. We calculated overall accuracy and Cohen's kappa for overall performance, and precision (producer's accuracy), recall (user's accuracy) and f1 score for individual class performance (Olofsson *et al* 2014). We calculated class confusion in a confusion matrix. We extracted the classified results for each validation point and calculated the accuracy metrics with the scikit-learn package (Pedregosa *et al* 2011).

From the final classification data, we calculated simple landscape metrics to identify landscape fragmentation and patch shape patterns. The area covered by each class (class area) and the arithmetic mean of patch sizes per class (mean patch size) are reported in hectare (ha). Total edge length per class area (edge density) is reported in m m^{-2}, with low edge density values representing circular shapes and higher values indicating more complex shapes.

4. Results

4.1. Vegetation and microtopography

Vegetation composition and cover varied markedly along the drainage age sequence (figure 3). The first principal component (PC1) reflected local hydrology, mainly submerged, wet, and moist situations (figure 4(a)). PC2 was linked to mature vegetation (emergent aquatic, moist dwarf shrub) versus wet tundra and pioneers. Accordingly, water depth correlated significantly with PCA results ($p = 0.008$, S2). Methane concentrations also correlated significantly ($p = 0.068$) with PCA results, with higher values in wetter plots (figure 4(a)), as did TOC/TN ratios ($p = 0.003$) and $\delta^{13}C$ ($p = 0.056$), which both showed higher values in moist raised plots beneath mature vegetation.

Clustering results supported those of PCA, differentiating vegetation composition in submerged plots from that in wet, moist, and pioneer plots (figure 4(b)). We identified five vegetation clusters (figure 4, table 1) that correspond to classes in the Circumpolar Arctic Vegetation Classification (Walker *et al* 2018). Table 1 lists taxa related to each cluster. Our aquatic wetland class represented pioneer fens in shallow water with *Arctophila fulva*. Emergent aquatics were dominated by *Carex aquatilis* and *Eriophorum angustifolium* in shallow water. Wet tundra, a diverse class dominated by *Carex stans*, was found in low-lying wet plots. The moist dwarf shrub class, on raised ice-wedge polygon rims, was most diverse. It was dominated by *Eriophorum vaginatum, C. stans*, and various dwarf shrubs and herbs. *Carex subspathacea* dominated the moist pioneer class, and was accompanied by *Salix* sp. and various herbs.

Ice-wedge polygon evolution was reflected in the microtopographic relief, which increased with drainage age (see figure 5(a)). Differences in relative ground surface height within the 10 m sub-transects increased from 9 cm in the recently drained basin

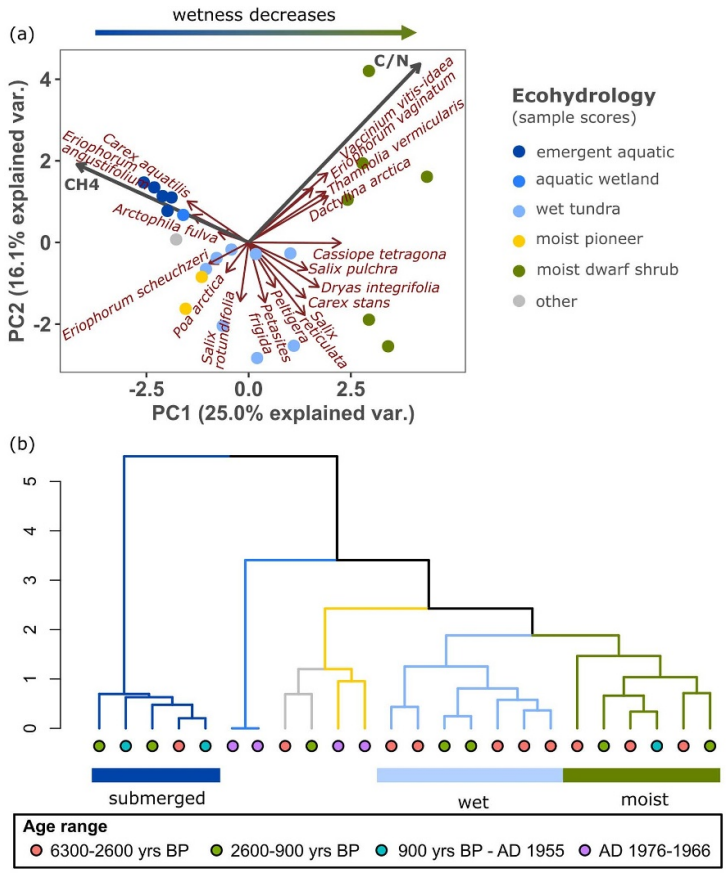

Figure 4. Ordination and clustering results of vascular plant and major lichen species composition and abundance. (a) Biplot showing results of the principal component analysis. Red arrows indicate species scores, sample score points are colour coded to the clustering results. Grey arrows indicate significant correlation ($p < 0.05$) of ordination results with sediment organic matter parameters. (b) Cluster dendrogram showing the results of hierarchical clustering. Colour coding of the branches refers to ecohydrological classes. Drainage age ranges are shown as colour-coded circles for each plot.

Table 1. Overview over vegetation classes.

	Dominant	Accompanying	Rare
Emergent aquatic	*Carex aquatilis, Eriophorum angustifolium*	*Eriophorum scheuchzeri, Ranunculus pallasii*	
Aquatic wetland	*Arctophila fulva*	*Ranunculus gmelinii*	
Wet tundra	*Carex stans*	*Luzula confusa, Poa arctica, Salix reticulata, S. rotundifolia, S. pulchra, Dryas integrifolia, Petasites frigida, Saxifraga cernua, Sphagnum* sp.	*E. scheuchzeri, E. angustifolium, E. vaginatum, Vaccinium vitis-idaea, Dactylina arctica*
Moist dwarf shrub	*Eriophorum vaginatum, Carex stans*	*S. pulchra, S.reticulata, D. integrifolia, Cassiope tetragona, Ledum decumbens, V. vitis-idaea, Sphagnum* sp., *Dactylina arctica, Peltigera* sp., *Thamnolia vermicularis*	*Arctagrostis latifolia, E. scheuchzeri, Rubus chamaemorus, Pyrola grandiflora, Saxifraga cernua, S. nelsoniana, Senecio atropurpurea, Petasites frigida, Pedicularis capitata*
Moist pioneer	*Carex subspathacea*	*Poa arctica, Salix rotundifolia, Saxifraga hirculus, Stellaria longipes, E. scheuchzeri, C. stans, Arctophila fulva, S. pulchra, Rumex arcticus, Silene involucrata, Stellaria humifusa*	

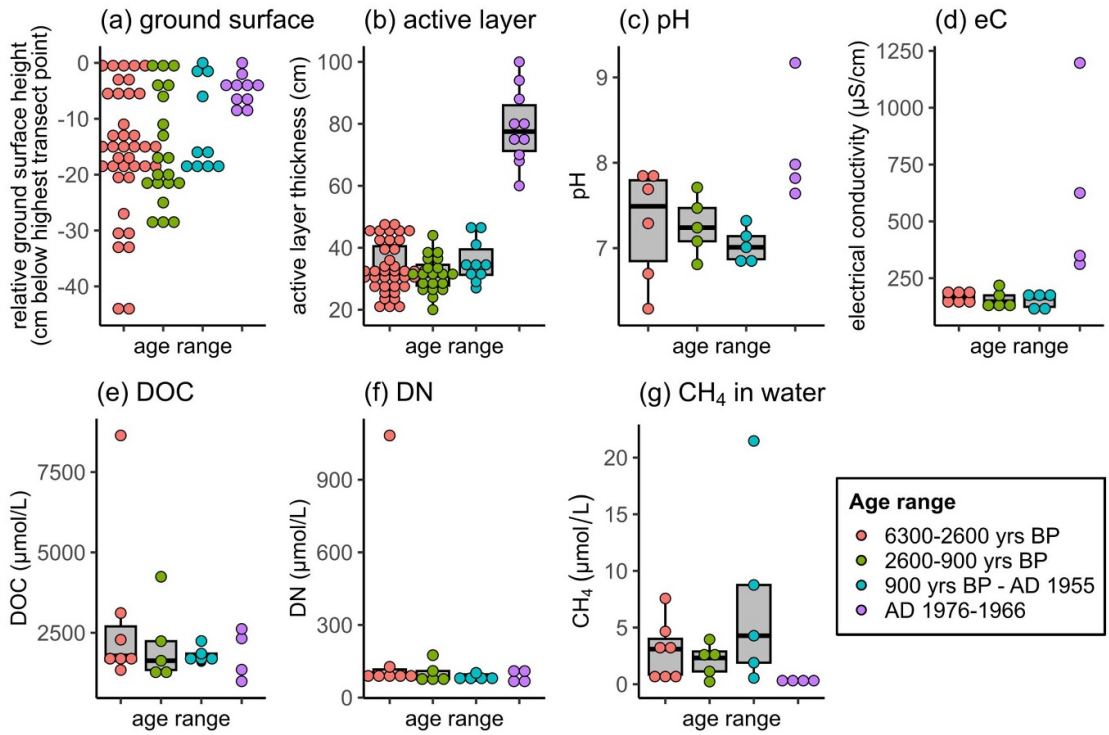

Figure 5. Microtopography and pond water parameters grouped by drainage age class: (a) relative ground surface height, (b) active layer thickness, (c) pH, (d) electrical conductivity, (e) dissolved organic carbon, (f) total dissolved nitrogen, (g) methane concentration in water. Point graphs indicate individual measurements and are colour coded to drainage age ranges. Boxplots are shown for groups with at least 5 measurements.

Table 2. Water and sediment parameters. Ranges and medians (M) are given for the youngest drainage age class, all older classes, and the total of all classes.

	Water					Sediment				
	pH	Electrical conductivity (μS cm^{-1})	DOC (μmol l^{-1})	TDN (μmol l^{-1})	CH4 (μmol l^{-1})	TOC (wt%)	TN (wt%)	TOC/TN	δ^{13}C (‰ vs. VPDB)	δ^{15}N (‰ vs. AIR)
Most recent AD 1966–1976	7.6–9.2 ($M = 7.9$)	312–1197 ($M = 487$)	990–2619 ($M = 1839$)	60–122 ($M = 86$)	0.1–0.5 ($M = 0.4$)	0.9–18.2 ($M = 6.2$)	<0.1–0.9 ($M = 0.5$)	17.9–19.5 ($M = 18.3$)	−30.4 to −25.4 ($M = -28.2$)	3.1–6.3 ($M = 3.1$)
All older 6300 BP-AD 1955	6.3–7.8 ($M = 7.2$)	108–218 ($M = 164$)	1206–8640 ($M = 1791$)	65–1083 ($M = 91$)	0.2–21.5 ($M = 2.6$)	38.8–46.3 ($M = 42.1$)	0.5–2.3 ($M = 1.5$)	18.6–83.8 ($M = 27.6$)	−30.8 to −25.0 ($M = -28.4$)	−1.0–2.1 ($M = 0.4$)
Total	**6.3–9.2 ($M = 7.3$)**	**108–1197 ($M = 173$)**	**990–8640 ($M = 1791$)**	**60–1083 ($M = 91$)**	**0.1–21.5 ($M = 1.5$)**	**0.9–46.3 ($M = 41.8$)**	**<0.1–2.3 ($M = 1.3$)**	**17.9–83.8 ($M = 26.2$)**	**−30.8 to −25.0 ($M = -28.4$)**	**−1.0–6.3 ($M = 0.4$)**

to 44 cm in the oldest age class. The active layer was much thicker and more variable in the recently drained basin (60–100 cm) compared to all other basin parts (20–46 cm) (figure 5(b)).

4.2. Water and sediment

The main patterns in water and sediment parameters were closely related to vegetation patterns: The most recently drained basin was markedly different from all older basins and submerged plots differed from moist plots. Wet plots were intermediary. In the basin that drained around AD 1966–1976, surface water bodies had higher pH and electrical conductivity than pre-1966 basin parts (figure 5, table 2). Surface sediments in this young basin had lower gravimetric TOC and TN, and lower water contents than in older age classes, while δ^{15}N was elevated (figure 6, table 2). Concentrations of CH_4 (0.1–21.5 μmol l^{-1}), DOC (990–8640 μmol l^{-1}), and TDN (60–1083 μmol l^{-1}) in pond water remained high and variable throughout and appeared to be independent of drainage age (figures 5(e)–(g), table 2). On the other hand, wetness was a good predictor of methane concentrations in sediment, which were significantly higher in submerged plots (25–200 μmol l^{-1}, $n = 5$) than in wet (3–61 μmol l^{-1}, $p = 0.03$, $n = 7$) or moist plots (1–18 μmol l^{-1}, $p = 0.0047$, $n = 9$) (figure 6, table 2).

4.3. Eco-hydrological land cover classification

We identified eight eco-hydrological land cover classes that corresponded to the five vegetation classes

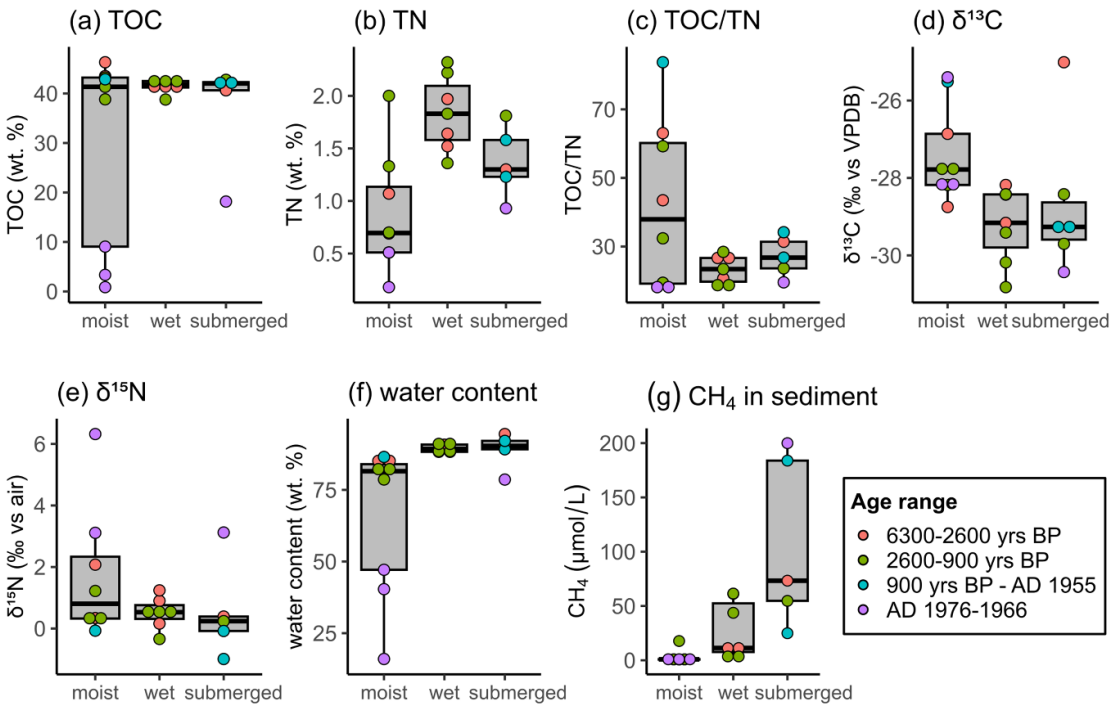

Figure 6. Sediment parameters grouped by main eco-hydrological setting: (a) total organic carbon, (b) total nitrogen, (c) organic carbon to nitrogen ratio, (d) stable carbon isotopes, (e) stable nitrogen isotopes, (f) water content, (g) methane concentration in sediment. Point graphs indicate individual measurements and are colour coded to drainage age ranges. Boxplots are shown for groups with at least five measurements.

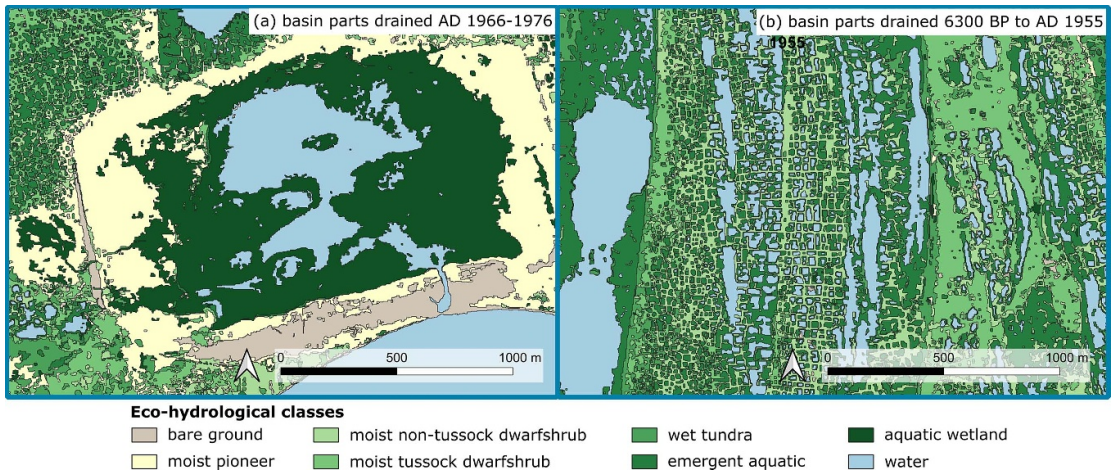

Figure 7. Close-ups of eco-hydrological land cover classification map produced in this study. The maps show large patches of pioneer and wet classes in the most recently drained basin (panel (a)) and small-scale heterogeneity of wet and moist patches caused by ice-wedge polygon development in basin parts that drained centuries to millennia ago (panel (b)).

we identified (figure 4), a water class and a bare ground class (figure 7). The moist dwarf shrub class we identified from vegetation data was subdivided into a tussock and a non-tussock class.

Accuracy assessment of the eco-hydrological land cover classification, based on stratified 5-fold cross-validation, achieved an overall accuracy of 68% and a kappa value of 0.63. Individual class performance varied strongly from water (F1 = 0.92) to wet tundra (F1 = 0.49). Most classes, except water, were affected by classification imbalance with differences between precision (producer's accuracy) and recall (user's accuracy). Particularly moist tussock dwarf shrub, with many patches falsely classified as this eco-hydrological class, and wet tundra, often classified as another class, showed strong imbalances. For detailed error analysis see confusion matrix (S3) and classification report (S4).

Methane concentrations differed between submerged, wet, and moist plots (figure 6), while drainage age best described differences in TOC, TN and δ^{15}N (figure 4). We therefore concentrated on

submerged versus wet and moist patches and drainage age to quantify spatial patterns relevant for upscaling. Submerged patches are occupied by emergent aquatics and aquatic wetlands. Wet patches are occupied by wet tundra, with a water table close to the ground surface. Moist patches, with a water table below ground, are occupied by moist pioneer, moist non-tussock dwarf shrub, and moist tussock dwarf shrub tundra.

We found that more area was occupied by submerged patches and water bodies (1055 ha, 42%) with very high methane concentrations than by moist patches and bare ground (885 ha, 35%) with low methane concentrations. Wet patches with intermediate methane concentrations occupied 565 ha (23%). Submerged patches and water bodies decreased from 46%–57% in the four youngest age classes to 12%–32% in the two oldest age classes. The submerged class aquatic wetland, representing pioneer fen vegetation, declined from 33% in the recently drained basin to less than 0.5% in all other age classes. Bare ground had its largest area in the youngest drainage age class (18 ha, 5%) and was otherwise low (0.1–5 ha, 0.2%–2.4%). This is in agreement with exposure of former lake sediment upon drainage followed by recolonization of almost all bare ground. We found larger patches (mean patch size = 0.5 ha) with simpler shapes (edge density = 808) in the youngest age class, and smaller patch sizes (mean patch size = 0.1–0.2 ha) accompanied by higher patch shape complexity (edge density = 1473–2171) in all other age classes. This pattern of increasing shape complexity and decreasing patch sizes with drainage age accompanied the increase in microtopographic complexity (figure 5), and was linked to ice-wedge polygon development.

5. Discussion

5.1. Vegetation and microtopography

We found that hydrological setting (PC1) was the main predictor of vegetation composition. This is typical for permafrost-affected wetlands because of local decimetre-scale differences in ground surface height (Wolter *et al* 2016), which increase with drainage age (figure 5). These microtopographic variations are mainly caused by ice wedge formation and their polygonal surface expressions (Mackay and Burn 2002). Submerged and moist patches can therefore be distinguished based on their characteristic vegetation. The second predictor of variability was linked to disturbance through lake drainage, vegetation succession and possibly nutrient availability (PC2). Overall, PC1 and PC2 explained 41% of the variation in vegetation data, and additional factors such as ground disturbance or nutrient availability, but also data limitations could play a role. Ground disturbance is a prominent driver of vegetation change in tundra with continuous vegetation cover (Myers-Smith *et al* 2011). Nutrient availability is another factor influencing vegetation composition and promoting rapid re-vegetation of drained lake beds (Ovenden 1986). Subsequent replacement of the pioneer *A. fulva* by *C. aquatilis* and *E. angustifolium* was also reported from northeastern Siberia (Li *et al* 2017) and northern Alaska (Billings and Peterson 1980). Loiko *et al* (2020) proposed that a major switch happens about 100–300 years after lake drainage, when mature vegetation is established. Our data corroborate that finding: In older basin parts, vegetation composition mainly traced differences in local hydrology.

5.2. Water and sediment organic matter

Dissolved organic matter derived from actively thawing permafrost can be highly biolabile (Vonk *et al* 2015). We found that pond water DOC (M = 27.2 mg l^{-1}, n = 21) was twice as high as lake DOC from the circum-Arctic (M = 10.8 mg l^{-1}) (Stolpmann *et al* 2021, n = 1833). Townsend-Small *et al* (2017) measured much lower summer DOC (M = 4.6 mg l^{-1}, n = 49) and TDN (M = 0.2 mg l^{-1}, n = 49 vs our 2.6 mg l^{-1}, n = 21) from lakes in our study region. Our findings support the importance of small and abundant water bodies in lowland permafrost (Muster *et al* 2017) for organic matter cycling, likely also for recycling other formerly freeze-locked elements like nitrogen or iron (Patzner *et al* 2020, Voigt *et al* 2020, Strauss *et al* 2022).

The very high sediment water contents (>79%) in all but the youngest class are consistent with published ice contents of 82% for drained lakes in the region (Kanevskiy *et al* 2013). Such water-saturated sediments with largely anoxic conditions have a high methane production potential (Garcia *et al* 2000, Knoblauch *et al* 2018), and our study found high sediment methane concentrations independent of drainage age (figure 6). Summer methane concentrations in ponds from our study were about 27 times higher than those reported from lakes in Arctic Alaska (Townsend-Small *et al* 2017), and were comparable to Alaskan lakes further south (Sepulveda-Jauregui *et al* 2015). Not all methane in sediment and pond water will be emitted to the atmosphere. A substantial portion is oxidised (Liebner *et al* 2011) before reaching the atmosphere as carbon dioxide. However, *in-situ* chamber experiments from north Alaska (Zona *et al* 2016) and northeast Siberia (van der Molen *et al* 2007) indicate elevated release of greenhouse gases from Arctic DLB wetlands.

Sediment properties (e.g. TOC, TOC/TN) in the recently drained basin are within expected ranges for lake sediments (Sepulveda-Jauregui *et al* 2015, Wolter *et al* 2017). In older basin parts, surface sediment composition indicated peat (figure 6) and differed primarily by eco-hydrological class. Differences between age classes relate to (i) surface peat thickness, which increases with basin age (Fuchs *et al* 2019) and

(ii) the area covered by each eco-hydrological class (figure 7).

5.3. Eco-hydrological land cover classification

We found that eco-hydrological class area can be detected and quantified using high-resolution optical satellite imagery (figure 7). Especially the submerged versus moist patch distinction, which explained vegetation variability (figure 4) and sediment methane concentration (figure 6), was well discerned. Accuracy assessments indicate that our land cover classification tended to underestimate submerged and wet surfaces while overestimating moist patches. Our interpretation is therefore conservative, with the true share of submerged patches with elevated methane concentrations likely being higher than our estimates. Hydrological conditions vary spatially within and between basins (Hinkel *et al* 2003, Loiko *et al* 2020). Towards the older parts of our drainage gradient, wet patches were smaller, while moist patches increased in size and shape complexity (figure 7). This development is linked to evolving ice-wedges, which create interconnected moist raised surfaces around wet depressions (Wolter *et al* 2016, 2018, French 2017). Such small-scale heterogeneity poses problems in simulations of regional to arctic-wide carbon dynamics, and needs to be accounted for (Lara *et al* 2020). High spatial mixing of interwoven patches may affect greenhouse gas fluxes from lowland tundra (Sturtevant and Oechel 2013). Increased connectivity between microhabitats facilitates species dispersal in tundra ecosystems (Dobbert *et al* 2021) and will have two effects under climatic warming: It might increase adaptability and resilience to environmental change, as species move to close-by more suitable habitat. It can also facilitate shrub expansion (Myers-Smith *et al* 2011), thereby altering physical landscape properties (Lantz *et al* 2010) and affecting the carbon cycle (Mekonnen *et al* 2021). Our study indicates that remote sensing-based eco-hydrological classes can be useful in upscaling efforts, with some limitations that still need to be addressed: More ground truth data needs to be obtained especially from pioneer classes and from different lowland permafrost regions. Lake drainage typically creates very diverse landscapes with a mosaic of basins of different drainage ages and high spatial heterogeneity.

6. Conclusions

Our findings demonstrate that vegetation composition is an important predictor of surface wetness in Arctic DLBs, which in turn drives sediment properties such as methane concentrations. We suggest that this relationship can be used to quantify submerged patches, and therefore areas with high sediment methane concentrations using high-resolution multispectral satellite imagery (figure 7). We found that DLBs are highly productive systems overall and most sediment parameters and organic matter in pond waters (DOC, DN, CH4) are very high independent of drainage age (figures 5 and 6). Our results indicate that differences between plots are better explained by their microtopographic position above, at, or below the water table than by basin age. Methane production in particular does not appear to decrease over time in the basins (figure 5), and we suggest additional research to investigate that question in more detail. The evolution of vegetation and ground ice formation-driven microtopography alters local surface wetness and thereby sediment parameters on small spatial scales (figures 5–7). We therefore suggest that larger scale investigations of vegetation, carbon and nitrogen dynamics in DLBs need to consider this small-scale variability in assessments of permafrost region contributions to global budgets.

Data availability statement

The data that support the findings of this study are partially available in the supplementary material, and will be openly available on the data repository PANGAEA following a delay.

Acknowledgments

We would like to thank our pilot Jim Webster for his invaluable help in the field, his calm and positive manner and his friendship. We would also like the thank three anonymous referees for the time and effort they put into reviewing this manuscript. Their constructive comments helped to improve the clarity and quality of this study. Field work was supported by ERC PETA-CARB (#338335). AWI LK-II funds facilitated the ThawTrendAir airborne imaging campaign with the Polar-6 airplane and the German Aerospace Centre allowed use of their modular aerial camera system (MACS). J W was funded by DFG Grant WO 2420/2-1. B J declares funding by U.S. National Science Foundation (NSF) Grants OPP-1806213 and OIA-1929170.

Conflict of interest

All authors declare that they have no conflict of interest.

ORCID iDs

Juliane Wolter https://orcid.org/0000-0001-6179-7621
Benjamin M Jones https://orcid.org/0000-0002-1517-4711
Matthias Fuchs https://orcid.org/0000-0003-3529-8284
Ingeborg Bussmann https://orcid.org/0000-0002-1197-7461

Boris Koch https://orcid.org/0000-0002-8453-731X
Josefine Lenz https://orcid.org/0000-0002-4050-3169
Isla H Myers-Smith https://orcid.org/0000-0002-8417-6112
Torsten Sachs https://orcid.org/0000-0002-9959-4771
Jens Strauss https://orcid.org/0000-0003-4678-4982
Ingmar Nitze https://orcid.org/0000-0002-1165-6852
Guido Grosse https://orcid.org/0000-0001-5895-2141

References

Andresen C G, Lara M J, Tweedie C E and Lougheed V L 2017 Rising plant-mediated methane emissions from Arctic wetlands *Glob. Change Biol.* **23** 1128–39
Billings W D and Peterson K M 1980 Vegetational change and ice-wedge polygons through the thaw-lake cycle in Arctic Alaska *Arct. Alp. Res.* **12** 413–32
Bockheim J G, Everett L R, Hinkel K M, Nelson F E and Brown J 1999 Soil organic carbon storage and distribution in Arctic tundra, barrow, Alaska *Soil Sci. Soc. Am. J.* **63** 934–40
Bussmann I, Fedorova I, Juhls B, Overduin P P and Winkel M 2021 Methane dynamics in three different Siberian water bodies under winter and summer conditions *Biogeosciences* **18** 2047–61
Davidson S J, Sloan V L, Phoenix G K, Wagner R, Fisher J P, Oechel W C and Zona D 2016 Vegetation type dominates the spatial variability in CH4 emissions across multiple Arctic tundra landscapes *Ecosystems* **19** 1116–32
Dobbert S, Pape R and Löffler J 2021 How does spatial heterogeneity affect inter- and intraspecific growth patterns in tundra shrubs? *J. Ecol.* **109** 4115–31
Edwards M, Grosse G, Jones B M and McDowell P 2016 The evolution of a thermokarst-lake landscape: late quaternary permafrost degradation and stabilization in interior Alaska *Limnol. Process. Permafr. Environ.* **340** 3–14
Engram M, Walter Anthony K M, Sachs T, Kohnert K, Serafimovich A, Grosse G and Meyer F J 2020 Remote sensing northern lake methane ebullition *Nat. Clim. Change* **10** 511–7
French H M 2017 *The Periglacial Environment* 4th edn (Wiley)
Fritz M, Wolter J, Rudaya N, Palagushkina O, Nazarova L, Obu J, Rethemeyer J, Lantuit H and Wetterich S 2016 Holocene ice-wedge polygon development in northern Yukon permafrost peatlands (Canada) *Quat. Sci. Rev.* **147** 279–97
Fuchs M, Lenz J, Jock S, Nitze I, Jones B M, Strauss J, Günther F and Grosse G 2019 Organic carbon and nitrogen stocks along a thermokarst lake sequence in Arctic Alaska *J. Geophys. Res.: Biogeosci.* **124** 1230–47
Garcia J-L, Patel B K C and Ollivier B 2000 Taxonomic, phylogenetic, and ecological diversity of methanogenic archaea *Anaerobe* **6** 205–26
Grosse G, Jones B M and Arp C D 2013 Thermokarst lakes, drainage, and drained basins *Treatise on Geomorphology* ed J F Shroder (Elsevier; USGS Publications Warehouse) vol 8 pp 325–53
Heslop J K, Walter Anthony K M, Sepulveda-Jauregui A, Martinez-Cruz K, Bondurant A, Grosse G and Jones M C 2015 Thermokarst lake methanogenesis along a complete talik profile *Biogeosciences* **12** 4317–31
Heslop J K, Walter Anthony K M, Winkel M, Sepulveda-Jauregui A, Martinez-Cruz K, Bondurant A, Grosse G and Liebner S 2020 A synthesis of methane dynamics in thermokarst lake environments *Earth Sci. Rev.* **210** 103365
Hinkel K M, Eisner W R, Bockheim J G, Nelson F E, Peterson K M and Dai X 2003 Spatial extent, age, and carbon stocks in drained thaw lake basins on the barrow peninsula, Alaska *Arctic Antarct. Alpine Res.* **35** 291–300
Hinkel K M, Frohn R C, Nelson F E, Eisner W R and Beck R A 2005 Morphometric and spatial analysis of thaw lakes and drained thaw lake basins in the western Arctic coastal plain, Alaska *Permafr. Periglac. Process.* **16** 327–41
Hinkel K M, Jones B M, Eisner W R, Cuomo C J, Beck R A and Frohn R 2007 Methods to assess natural and anthropogenic thaw lake drainage on the western Arctic coastal plain of northern Alaska *J. Geophys. Res.* **112** F02S16
Hugelius G *et al* 2014 Estimated stocks of circumpolar permafrost carbon with quantified uncertainty ranges and identified data gaps *Biogeosciences* **11** 6573–93
IPCC 2022 Climate change 2022: impacts, adaptation, and vulnerability *Contribution of Working Group II to the Sixth Assessment Report of the Intergovernmental Panel on Climate Change* ed H-O Pörtner, D C Roberts, M Tignor, E S Poloczanska, K Mintenbeck, A Alegría, M Craig, S Langsdorf, S Löschke, V Möller, A Okem and B Rama (Cambridge University Press)
Jafarov E E, Parsekian A D, Schaefer K, Liu L, Chen A C, Panda S K and Zhang T 2017 Estimating active layer thickness and volumetric water content from ground penetrating radar measurements in Barrow, Alaska *Geosci. Data J.* **4** 72–79
Jones B M *et al* 2022 Lake and drained lake basin systems in lowland permafrost regions *Nat. Rev. Earth Environ.* **3** 85–98
Jones B M and Arp C D 2015 Observing a catastrophic thermokarst lake drainage in Northern Alaska *Permafr. Periglac. Process.* **26** 119–28
Jones M C, Grosse G, Jones B M and Walter Anthony K 2012 Peat accumulation in drained thermokarst lake basins in continuous, ice-rich permafrost, northern Seward Peninsula, Alaska *J. Geophys. Res.: Biogeosci.* **117**
Jorgenson M T and Shur Y 2007 Evolution of lakes and basins in northern Alaska and discussion of the thaw lake cycle *J. Geophys. Res.* **112**
Kanevskiy M, Shur Y, Jorgenson M T, Ping C-L, Michaelson G J, Fortier D, Stephani E, Dillon M and Tumskoy V 2013 Ground ice in the upper permafrost of the Beaufort Sea coast of Alaska *Cold Reg. Sci. Technol.* **85** 56–70
Knoblauch C, Beer C, Liebner S, Grigoriev M N and Pfeiffer E-M 2018 Methane production as key to the greenhouse gas budget of thawing permafrost *Nat. Clim. Change* **8** 309–12
Kokelj S V and Jorgenson M T 2013 Advances in thermokarst research *Permafr. Periglac. Process.* **24** 108–19
Langer M, Westermann S, Boike J, Kirillin G, Grosse G, Peng S and Krinner G 2016 Rapid degradation of permafrost underneath waterbodies in tundra landscapes—toward a representation of thermokarst in land surface models *J. Geophys. Res.* **121** 2446–70
Lantz T C, Gergel S E and Kokelj S V 2010 Spatial Heterogeneity in the shrub tundra ecotone in the mackenzie delta region, northwest territories: implications for Arctic environmental change *Ecosystems* **13** 194–204
Lara M J, McGuire A D, Euskirchen E S, Genet H, Yi S, Rutter R, Iversen C, Sloan V and Wullschleger S D 2020 Local-scale Arctic tundra heterogeneity affects regional-scale carbon dynamics *Nat. Commun.* **11** 4925
Li B, Heijmans M M P D, Blok D, Wang P, Karsanaev S V, Maximov T C, van Huissteden J and Berendse F 2017 Thaw pond development and initial vegetation succession in experimental plots at a Siberian lowland tundra site *Plant Soil.* **420** 147–62
Liebner S, Zeyer J, Wagner D, Schubert C, Pfeiffer E-M and Knoblauch C 2011 Methane oxidation associated with submerged brown mosses reduces methane emissions from Siberian polygonal tundra *J. Ecol.* **99** 914–22
Ling F and Zhang T 2004 Modeling study of talik freeze-up and permafrost response under drained thaw lakes

on the Alaskan Arctic Coastal Plain *J. Geophys. Res. Atmos.* **109**

Loiko S, Klimova N, Kuzmina D and Pokrovsky O S 2020 Lake drainage in permafrost regions produces variable plant communities of high biomass and productivity *Plants* **9** 867

Mackay J R 1988 Catastrophic lake drainage, tuktoyaktuk peninsula area, district of mackenzie *Curr. Res.* D **88** 83–90

Mackay J R 1999 Periglacial features developed on the exposed lake bottoms of seven lakes that drained rapidly after 1950, tuktoyaktuk peninsula area, western arctic coast, Canada *Permafr. Periglac. Process.* **10** 39–63

Mackay J R and Burn C R 2002 The first 20 years (1978-1979–1998–1999) of ice-wedge growth at the Illisarvik experimental drained lake site, western Arctic coast, Canada *Can. J. Earth Sci.* **39** 95–111

Magen C, Lapham L L, Pohlman J W, Marshall K, Bosman S, Casso M and Chanton J P 2014 A simple headspace equilibration method for measuring dissolved methane *Limnol. Oceanogr.* **12** 637–50

Mekonnen Z A *et al* 2021 Arctic tundra shrubification: a review of mechanisms and impacts on ecosystem carbon balance *Environ. Res. Lett.* **16** 053001

Mishra U *et al* 2021 Spatial heterogeneity and environmental predictors of permafrost region soil organic carbon stocks *Sci. Adv.* **7** eaaz5236

Muster S *et al* 2017 PeRL: a circum-Arctic permafrost region pond and lake database *Earth Syst. Sci. Data* **9** 317–48

Myers-Smith I H *et al* 2011 Shrub expansion in tundra ecosystems: dynamics, impacts and research priorities *Environ. Res. Lett.* **6** 045509

Olefeldt D *et al* 2016 Circumpolar distribution and carbon storage of thermokarst landscapes *Nat. Commun.* **7** 13043

Olofsson P, Foody G M, Herold M, Stehman S V, Woodcock C E and Wulder M A 2014 Good practices for estimating area and assessing accuracy of land change *Remote Sens. Environ.* **148** 42–57

Ovenden L 1986 Vegetation colonizing the bed of a recently drained thermokarst lake (Illisarvik), Northwest Territories *Can. J. Bot.* **64** 2688–92

Patzner M S *et al* 2020 Iron mineral dissolution releases iron and associated organic carbon during permafrost thaw *Nat. Commun.* **11** 6329

Pedregosa F *et al* 2011 Scikit-learn: machine learning in python *J. Mach. Learn. Res.* **12** 2825–30

R Core Team 2021 R: a language and environment for statistical computing Software (R Foundation for Statistical Computing) (available at: www.R-project.org/)

Regmi P, Grosse G, Jones M C, Jones B M and Anthony K W 2012 Characterizing post-drainage succession in thermokarst lake basins on the Seward peninsula, Alaska with TerraSAR-X backscatter and landsat-based NDVI data *Remote Sens.* **4** 3741–65

Rettelbach T *et al* 2023 Super-high-resolution aerial imagery datasets of permafrost landscapes in Alaska and northwestern Canada *Earth Syst. Sci. Data Discuss.* **2023** 1–35

Reuss-Schmidt K, Levy P, Oechel W, Tweedie C, Wilson C and Zona D 2019 Understanding spatial variability of methane fluxes in Arctic wetlands through footprint modelling *Environ. Res. Lett.* **14** 125010

Schädel C *et al* 2016 Potential carbon emissions dominated by carbon dioxide from thawed permafrost soils *Nat. Clim. Change* **6** 950–3

Sepulveda-Jauregui A, Walter Anthony K M, Martinez-Cruz K, Greene S and Thalasso F 2015 Methane and carbon dioxide emissions from 40 lakes along a north–south latitudinal transect in Alaska *Biogeosciences* **12** 3197–223

Stolpmann L *et al* 2021 First pan-Arctic assessment of dissolved organic carbon in lakes of the permafrost region *Biogeosciences* **18** 3917–36

Strauss J *et al* 2022 A globally relevant stock of soil nitrogen in the Yedoma permafrost domain *Nat. Commun.* **13** 6074

Sturtevant C S and Oechel W C 2013 Spatial variation in landscape-level CO2 and CH4 fluxes from Arctic coastal tundra: influence from vegetation, wetness, and the thaw lake cycle *Glob. Change Biol.* **19** 2853–66

Townsend-Small A, Åkerström F, Arp C D and Hinkel K M 2017 Spatial and temporal variation in methane concentrations, fluxes, and sources in lakes in Arctic Alaska *J. Geophys. Res.: Biogeosci.* **122** 2966–81

Treat C C *et al* 2016 Effects of permafrost aggradation on peat properties as determined from a pan-Arctic synthesis of plant macrofossils *J. Geophys. Res.: Biogeosci.* **121** 78–94

Ulrich M, Grosse G, Strauss J and Schirrmeister L 2014 Quantifying wedge-ice volumes in yedoma and thermokarst basin deposits *Permafr. Periglac. Process.* **25** 151–61

van der Molen M K, van Huissteden J, Parmentier F J W, Petrescu A M R, Dolman A J, Maximov T C, Kononov A V, Karsanaev S V and Suzdalov D A 2007 The growing season greenhouse gas balance of a continental tundra site in the Indigirka lowlands, NE Siberia *Biogeosciences* **4** 985–1003

Verville J H, Hobbie S E, Chapin F S and Hooper D U 1998 Response of tundra CH4 and CO2 flux tomanipulation of temperature and vegetation *Biogeochemistry* **41** 215–35

Voigt C, Marushchak M E, Abbott B W, Biasi C, Elberling B, Siciliano S D, Sonnentag O, Stewart K J, Yang Y and Martikainen P J 2020 Nitrous oxide emissions from permafrost-affected soils *Nat. Rev. Earth Environ.* **1** 420–34

von Fischer J C, Rhew R C, Ames G M, Fosdick B K and von Fischer P E 2010 Vegetation height and other controls of spatial variability in methane emissions from the Arctic coastal tundra at Barrow, Alaska *J. Geophys. Res.: Biogeosci.* **115**

Vonk J E *et al* 2015 Reviews and syntheses: effects of permafrost thaw on Arctic aquatic ecosystems *Biogeosciences* **12** 7129–67

Walker D A *et al* 2018 Circumpolar Arctic vegetation classification *Phytocoenologia* **48** 181–201

Walter K M, Smith L C and Stuart Chapin F 2007 Methane bubbling from northern lakes: present and future contributions to the global methane budget *Phil. Trans. R. Soc.* A **365** 1657–76

Wolter J, Lantuit H, Fritz M, Macias-Fauria M, Myers-Smith I and Herzschuh U 2016 Vegetation composition and shrub extent on the Yukon coast, Canada, are strongly linked to ice-wedge polygon degradation *Polar Res.* **35** 27489

Wolter J, Lantuit H, Herzschuh U, Stettner S and Fritz M 2017 Tundra vegetation stability versus lake-basin variability on the yukon coastal plain (NW Canada) during the past three centuries *Holocene* **27** 1846–58

Wolter J, Lantuit H, Wetterich S, Rethemeyer J and Fritz M 2018 Climatic, geomorphologic and hydrologic perturbations as drivers for mid- to late Holocene development of ice-wedge polygons in the western Canadian Arctic *Permafr. Periglac. Process.* **29** 164–81

Zona D *et al* 2016 Cold season emissions dominate the Arctic tundra methane budget *Proc. Natl Acad. Sci.* **113** 40–45

Zona D, Oechel W C, Kochendorfer J, Paw U, K T, Salyuk A N, Olivas P C, Oberbauer S F and Lipson D A 2009 Methane fluxes during the initiation of a large-scale water table manipulation experiment in the Alaskan Arctic tundra *Glob. Biogeochem. Cycles* **23**